LBL-17266
Preprint c.2

Lawrence Berkeley Laboratory
UNIVERSITY OF CALIFORNIA

RECEIVED
LAWRENCE
BERKELEY LABORATORY
APR 17 1984
LIBRARY AND
DOCUMENTS SECTION

Submitted to Physical Review C

A HIGH RESOLUTION STUDY OF THE BREAKUP OF ^{16}O AND ^{20}Ne AT 9 MeV/A

W.D.M. Rae, A.J. Cole, B.G. Harvey, and
R.G. Stokstad

March 1984

TWO-WEEK LOAN COPY
This is a Library Circulating Copy which may be borrowed for two weeks. For a personal retention copy, call Tech. Info. Division, Ext. 6782.

NUCLEAR SCIENCE DIVISION

LBL-17266 c.2

Prepared for the U.S. Department of Energy under Contract DE-AC03-76SF00098

DISCLAIMER

This document was prepared as an account of work sponsored by the United States Government. While this document is believed to contain correct information, neither the United States Government nor any agency thereof, nor the Regents of the University of California, nor any of their employees, makes any warranty, express or implied, or assumes any legal responsibility for the accuracy, completeness, or usefulness of any information, apparatus, product, or process disclosed, or represents that its use would not infringe privately owned rights. Reference herein to any specific commercial product, process, or service by its trade name, trademark, manufacturer, or otherwise, does not necessarily constitute or imply its endorsement, recommendation, or favoring by the United States Government or any agency thereof, or the Regents of the University of California. The views and opinions of authors expressed herein do not necessarily state or reflect those of the United States Government or any agency thereof or the Regents of the University of California.

LBL-17266

A HIGH RESOLUTION STUDY OF THE BREAKUP OF ^{16}O and ^{20}Ne at 9 MeV/A

W. D. M. Rae[+],

Nuclear Physics Laboratory,
Oxford, England
and
Nuclear Science Division
Lawrence Berkeley Laboratory
University of California
Berkeley, California 94720

A. J. Cole[++], B. G. Harvey and R. G. Stokstad

Nuclear Science Division
Lawrence Berkeley Laboratory
University of California
Berkeley, California 94720

Abstract

A high resolution study of the breakup of ^{16}O and ^{20}Ne has been made at 9 MeV per nucleon. The experimental configuration preferentially detects sequential breakup events. The dominant source of α-^{12}C and α-^{16}O coincidence events is the decay of excited states in ^{16}O and ^{20}Ne, respectively. The experimental technique and the reaction mechanism leading to sequential breakup are discussed.

+ Permanent address: Nuclear Physics Laboratory, Oxford, England.

++ Permanent address: Institut des Sciences Nucléaires, Grenoble, France.

1. Introduction

Over the last few years there have been many experimental investigations of heavy-ion breakup yielding both inclusive and coincidence data [1-10] on a wide range of targets over a wide range of energies. These experimental investigations have been spurred by considerable theoretical interest in the reaction mechanism and in the evolution of heavy-ion reactions with bombarding energy [11-17].

Inclusive measurements, while valuable in investigating global dependences of heavy-ion reactions on energy, angle and Q-value, do not provide conclusive evidence on mechanisms. Coincidence experiments are expected to yield much more detailed information on the reaction mechanism. A problem, however, is that coincidence experiments can be too specific: they may cover only small regions of the phase space available to the final state. Indeed, several reaction mechanisms may be involved [7, 18-21] in the production of light particles in coincidence with heavy fragments. One of these mechanisms, called sequential breakup, has been clearly identified by several high resolution coincidence experiments [4, 5, 22-25]. In sequential breakup, projectile-like nuclei are formed in particle unstable states that subsequently decay into a heavy fragment and a light fragment. The latter is usually an alpha particle or proton although neutrons would also be expected. In a few cases [4, 9, 22, 23] it has been shown that sequential decay is responsible for a large part of the coincidence cross section and that it contributes heavily to the inclusive ejectile yields [4, 9]. It is still an open question to what extent this conclusion is valid when the ejectile is much lighter than the projectile, or when the beam energy is substantially higher than 20 MeV/A.

In this paper we address the problem of attaining a better understanding of the sequential component. A good understanding of this component is necessary to enable it to be identified and separated from other mechanisms.

We describe an experimental technique which is specifically suited to study this component. Consequently we cannot address more global questions, such as the relative importance of this component to other mechanisms. However, our data, which have high energy and angular resolution, do allow us to reach some definite conclusions on the mechanisms leading to the sequential component and also on the dependence of this component on energy, angle and Q-value.

In this paper we present the experimental technique in detail and an overview of the data for reactions induced by ^{16}O on targets of ^{12}C, ^{13}C and ^{28}Si at 140 MeV and for reactions induced by ^{20}Ne on a ^{12}C target at 175 MeV. A more detailed analysis of some of these data along the lines of ref. [26] will follow in subsequent papers.

The experimental details are described in section 2. The ^{16}O induced reactions are discussed in section 3.1 and those induced by ^{20}Ne in section 3.2 We present our conclusions and discussion in section 4.

2. Experimental Method and Data Reduction

2.1 Experimental Setup

The oxygen and neon beams were provided by the Lawrence Berkeley Laboratory 88-Inch Cyclotron. Solid, self supporting targets of natural carbon (275μg/cm^2), ^{13}C enriched to 99% (285μg/cm^2) and ^{28}Si (500μg/cm^2) were used. Light particles (alpha particles and protons) were detected in coincidence with heavy ions in a position-sensitive detector telescope consisting of a 185μm Si ΔE detector and a 4970μm Si(Li) E detector (see figure 1). This telescope also recorded the horizontal position (E detector) and the vertical position (ΔE detector) of the light ions. It had an active circular area of diameter 40 mm. The heavy-ion telescope consisted of a 40μm ΔE detector which recorded the horizontal position and a 1500μmE detector which recorded the vertical position. The active diameter of this telescope was 8mm. An aluminum

absorber foil (50mg/cm^2) placed in front of the light-ion telescope stopped elastically scattered particles. The absorber, combined with the thickness of the ΔE detector, effectively prevented particles with $Z>2$ from being recorded by this telescope. The light-ion and heavy-ion telescopes were placed at 20cm and 15cm from the target, respectively, on opposite sides of the beam. For ^{16}O on ^{12}C and ^{13}C, data were taken in two heavy-ion angle settings of 8.75° and 13°, with the center of the light-ion telescope at 10.5°. For ^{16}O on ^{28}Si, and ^{20}Ne on ^{12}C, data were taken for only one heavy-ion angle, viz 11°, with the light-ion telescope again at 10.5°.

The circular position-sensitive detectors [27] used in this experiment have a non-linear position response. To calibrate these devices, grids consisting of brass plates containing regularly spaced holes were placed in front of the detectors before and after the experiment. The position spectra obtained with the grids in place (see figure 2) and a calibration procedure using fifth order polynomials enabled the determination of the polar and azimuthal angles for each particle.

2.2 Kinematics

In this experiment the energies of the two particles are measured, namely E_{LI} and E_{HI}. Provided the reaction mechanism is predominantly ejectile breakup it is then convenient to transform the data to two other variables. The appropriate variables are the 3-body Q-value, Q_3, and the LI-HI relative kinetic energy, E_{rel}, in the rest frame of the excited ejectile. In terms of these variables the 3-body kinematics reduce to quasi two-body kinematics, which greatly simplifies an otherwise complicated problem. The 3-body reaction Q-value is calculated using conservation of momentum and energy assuming a 3-body final state. This approach is also valid for 4 or more body reactions if all undetected particles are considered together and assumed to correspond to a single residual nucleus with appropriate kinetic and excitation energies.

We have (non-relativistically)

$$\vec{P}_{recoil} + \vec{P}_{HI} + \vec{P}_{LI} = \vec{P}_{beam} \tag{1}$$

$$(K.E.)_{recoil} - (K.E.)_{HI} + (K.E.)_{LI} + Q_3 = (K.E.)_{beam} \tag{2}$$

The first equation can be used to calculate $(K.E.)_{recoil}$ and then the second equation defines Q_3. A schematic Q_3 spectrum is given in figure 3. For low values of Q_3 the peaks correspond to excited states in the recoil (undetected) nucleus. At more negative values of Q_3, peaks corresponding to bound states of the detected heavy ion appear. These are broadened due to gamma-ray decay in flight. Finally, at even more negative Q_3 values, excited states of the light ion could appear - again broadened by gamma-ray recoil.

The relative kinetic energy of the light and heavy ions can be obtained from a 3-body kinematic analysis of each event. The simplest approach is to calculate the relative velocity directly,

$$\vec{V}_{rel} = \vec{V}_{lab_{LI}} - \vec{V}_{lab_{HI}} \tag{3}$$

The cosine rule yields

$$E_{rel} = (1/(M_{LI} + M_{HI})) \times$$

$$[M_{HI} \times E_{lab_{LI}} + M_{LI} \times E_{lab_{HI}}$$

$$- 2\sqrt{M_{HI}\, M_{LI}\, E_{lab_{HI}}\, E_{lab_{LI}}} \times \cos \theta_{HL}]$$

where θ_{HL} is the angle in the laboratory between $\vec{V}_{LI}$ and $\vec{V}_{HI}$. A schematic E_{rel} spectrum is given in figure 4.

For events having all final particles in their ground states, i.e., corresponding to the first peak in the Q_3 spectrum and often referred to as Q_{ggg}, the excitation energy of the excited ejectile breakup is related to E_{rel} by

$$E_x = E_{rel} + E_{thresh} \tag{5}$$

where E_{thresh} is the threshold energy for breakup of that nucleus into the observed channel. For events corresponding to other peaks in the Q_3 spectrum there may be some ambiguity in E_x. For peaks in Q_3 for which

$$Q_{ggg}-Q_3 < E^*_{HI}$$

where E^*_{HI} is the first excited state of the heavy ion, equation (5) is valid and unique. For

$$Q_{ggg}-Q_3 \geq E^*_{HI}$$

there will generally be an ambiguity so that peaks in E_{rel} cannot be uniquely identified with excitation energy. This is illustrated schematically in figure 4b by the shaded peaks.

2.3 Energy Resolution

2.3.1 Random Errors

In this type of experiment the energy resolutions obtained for Q_3 and E_{rel} differ considerably. Since $Q_3 \approx E_{LI} + E_{HI} - E_{BEAM}$, all the usual contributions influence the Q_3 resolution. By differentiation and quadrature

$$(\Delta Q_3)^2 = (\Delta E_{LI})^2 + (\Delta E_{HI})^2 + (\Delta E_B)^2 \quad .$$

Hence, detector resolution, beam resolution, energy straggling in the target, effects of differential target thickness and kinematic shifts from beam spot size, and beam divergence all contribute approximately in quadrature to ΔQ_3. There may also be an additional contribution from the kinematic-shift arising from the finite position resolution of the detectors. Our Q_3 resolution is typically 750 KeV.

In contrast, for E_{rel} there are strong correlations between many of these errors and, it turns out, considerable cancellation of various contributions yielding resolutions of 100-300 KeV for E_{rel} in our experiment. First, E_{rel} by definition must be independent of beam resolution and beam divergence. Since

$$V_{rel}^2 = V_{LI}^2 + V_{HI}^2 - 2\, V_{LI}\, V_{HI} \cos \theta_{HL}, \tag{6}$$

then

$$V_{rel}\, dV_{rel} = V_{LI}\, dV_{LI} - V_{HI} \cos \theta_{HL}\, dV_{LI}. \tag{7}$$

With reference to figure 5 where two possible decay configurations are shown, for configuration a) we have $V_{HI} \cos\theta_{HL} \approx V_{LI}$. Hence $V_{rel} dV_{rel} << V_{LI} dV_{LI}$. Similarly we can obtain $V_{rel} dV_{rel} << V_{HI} dV_{HI}$. So the resolution for E_{rel} depends weakly on the resolution for E_{LI} and E_{HI} for configuration a). However the resolution for E_{rel} does depend on the accuracy of the measurement of θ_{HL}

$$dE_{rel} \sim \sqrt{M_{LI} M_{HI} E_{HI} E_{LI}}\ \sin \theta_{HL}\, d\theta_{HL} \tag{8}$$

For the second configuration shown in figure 5 a similar analysis shows that the θ_{HL} does not contribute so that the E_{rel} resolution is determined by the E_{LI} and E_{HI} resolutions.

Most of our data correspond to configuration a) of figure 5, so that θ_{HL} resolution is important. Hence position-sensitive detectors are needed. Simple calculations show that the θ_{HL} resolution is dominant in determining our E_{rel} resolution for most of the data. Note that θ_{HL} is not just the in-plane angle between $\vec{V}_{LI}$ and $\vec{V}_{HI}$. Thus, for detectors with significant height, a y position measurement is needed to get good θ_{HL} resolution. However for large θ_{HL} this out of plane angle enters only in second order ($\sim y^2/\theta_{HL}^2$).

The cancellation discussed above that reduces the contribution of the (random) detector resolution contributions to ΔE_{HI} and ΔE_{LI} and thus to ΔE_{rel} does not necessarily apply to correlated errors. Target-related resolution effects will have some degree of correlation. However, one can probably apply the above analysis to most of these effects also.

A complication in attempts to estimate the expected E_{rel} resolution arises from the dependence of the position resolution on the amount of energy deposited in the detector. This is most severe for the light-ion telescope where comparatively small energies are deposited in the detectors. It is important for light-ion energies encountered in configuration a) that one of the detectors in the light-ion telescope be able to detect alpha particles with energies as low as 5 MeV. This can put a constraint on the ΔE thickness and influence the choice of which detector (ΔE or E) measures the horizontal position. A final contribution to the E_{rel} resolution comes from the beam spot size. This can contribute to errors in θ_{HL} that cancel to first order for detectors equidistant from the target.

2.3.2 Systematic Errors

Various systematic errors can arise in the energies calculated in this experiment. These include errors originating with a ΔE-E miscalibration, E_{HI}-E_{α} miscalibration, dead layers in detectors, insufficient charge collection, ionization defects, energy loss in the

target, correction for energy loss in absorbers etc. We made all our relative calibrations with a pulser and a charge terminator. However, comparison of this calibration with that obtained using α sources revealed some of the above problems at the level of 0.5-1 MeV. These errors are exaggerated in the calculation of Q_3 and E_{rel}, making Q_3 and E_{rel} dependent on other variables. To overcome this problem, a small empirical correction of the form

$$E' = \alpha E + \beta(PI)/E^{0.7}$$

was applied after all other corrections had been made. The particle-identification signal is defined by

$$PI = k \sqrt{(\Delta E + E_r)^{1.7} - E_r^{1.7}} \propto A^{0.7}Z^2$$

The use of the PI signal in this formula makes the second term in the correction, determined by β, independent of particle type. The values of α and β were varied to make the Q_3 and E_{rel} peaks simultaneously independent of all other variables. Typically $\alpha \sim 0.98$ to 1.02. The value of β depends on the normalization of the PI signal.

In this paper the spectra were calculated without the above empirical adjustment. However the energies quoted are those obtained after this empirical correction. The most significant effect of this correction is on the resolution obtained in the experiment. It has a much smaller effect on the calibration.

This discussion reveals the importance of carefully correcting the light-ion energy for the energy lost in the absorber. In principle it would be best to avoid the use of an absorber. However in practice it allows a much higher coincidence rate using a very large light-ion telescope. Some of the energies we have quoted previously [22, 23] have been in error due to errors in the absorber correction procedure. For the data reported here a range-energy [28] lookup table was used to correct these energies.

2.4 Cross sections

In this paper we will present some angular distributions for the inelastic excitation of ^{16}O to the 11.52 MeV state which subsequently α decays. Fuchs [29] has discussed the general problems of coordinate and cross section transformations between different reference frames. Here we discuss a few points of relevance to our experimental setup.

Figure 6 defines the polar (and associated azimuthal) angles in this experiment relevant to a sequential decay mechanism. These are θ^*_{lab} (ϕ^*_{lab}), the laboratory angles of the excited nucleus before it decays (cf two body reactions) and $\psi(\chi)$ the angle of the relative velocity $\vec{V}_{rel}$ with respect to the beam (or ψ^* (χ^*) with respect to the ejectile direction in the laboratory). Corresponding to θ^*_{lab} (ϕ^*_{lab}) we have the angles θ^*_{cm} and ϕ^*_{cm}.

To calculate the double differential cross section in these variables the easiest way to proceed is to bin the events directly in terms of these variables. By conservation of number of events this must yield the correct answer. However, various "cuts" in the laboratory system, viz., detector boundaries and detector energy thresholds, result in complicated multi-dimensional cuts in the $\theta^*,\phi^*,\psi,\chi$ space. These boundaries must be determined and for those bins crossed by these boundaries the cross section obtained is meaningless. Only the bins which lie completely inside the boundaries will yield correct cross sections. Thus, this is a difficult task.

An alternative is to bin the data in the laboratory where the "cuts" are simple and easily handled. This method was used in the analysis here. The detectors were subdivided into vertical strips whose area is known. The double differential cross section was calculated for each pair of strips. (We are thus neglecting any out-of-plane dependence by averaging over the height of the strips). Event by event, we stored

for each pair of strips the number of counts, N, the polar angle of the excited ejectile, $\Sigma\theta_{cm}$, $\Sigma\theta_{cm}$, $\Sigma\psi^*$, $\Sigma\psi^{*2}$ and ΣJ where $J=J(\theta^*\phi^*,\psi^*\ \chi^*)$ is the Jacobian for the transformation from the variables $E_{HI}\theta_{HI}\phi_{HI}E_{LI}\theta_{LI}\phi_{LI}$ to E_{rel}, Q_3, θ^*,ϕ^*, ψ^*, χ^*, as given by Fuchs [29].

The cross section at $\langle\theta_{cm}\rangle = \Sigma\theta_{cm}/\Sigma N$ and $\langle\psi^*\rangle = \Sigma\psi^*/\Sigma N$ is then given by ΣJ, apart from the normal target and beam integration related factors. From $\langle\theta^{*2}\rangle$ and $\langle\psi^{*2}\rangle$ an estimate of the spread of the data points over these variables can be obtained. Finally, those cross sections with $\langle\psi^*\rangle$ close to the limiting values set by the energy and angle thresholds must be discarded. The relation between the energy and angle threshold and ψ^* is given in figure 7.

A disadvantage of this method is that the values $\langle\theta^*\rangle$, $\langle\psi^*\rangle$ obtained do not lie on a regular grid allowing easy manipulation or presentation of the final cross sections. This is a significant problem if large amounts of data are to be analyzed.

A compromise solution has been presented in ref. [26]. This involves two new main steps. One is the use of an axial coordinate system with the Z axis perpendicular to the reaction plane rather than a spherical coordinate system. The second change is that the Jacobian is approximated by the inplane Jacobian. (This is in addition to the neglect of out-of-plane effects as discussed above). The technique involves binning the data into θ_{AX} and ψ_{AX} directly in regular bins while using a Jacobian to transform the out-of-plane volume elements $d\phi_1 d\phi_2 \rightarrow d\phi^* d\chi$. Detector boundaries and energy cuts in the laboratory now only require the identification of a two dimensional boundary in the θ_{AX}- ψ_{AX} plane. This is a manageable problem. The only disadvantage of this technique is found at angles close to $\theta^* = 0^\circ$ (spherical). Here the axial coordinate system is unphysical. However, axial and spherical coordinate systems are almost identical in-plane away from 0°. Further details are to be found in ref. [26].

Both the above methods are approximately valid only in the in-plane limit. Both break down for detectors with significant height and for very small E_{rel} values and small θ_{HL}. However they have been checked with Monte-Carlo simulation and appear to be sufficiently accurate for most purposes.

3. Experimental Results

3.1 ^{16}O Induced Reactions

3.1.1 The breakup of ^{16}O into $^{12}C + \alpha$

In figure 8 we present Q_3 spectra for the breakup of ^{16}O into $^{12}C + \alpha$ on the three targets ^{12}C, ^{13}C and ^{28}Si for $\theta_\alpha = 10.5°$ and $\theta_{HI} = 8.75°$. These spectra show peaks corresponding to excited states of both the target and the detected ^{12}C ion. For more negative Q-values a continuum is observed on all targets. E_{rel} spectra are presented in figure 9 for events corresponding to $Q_{ggg} = -7.16$ MeV, which leaves all three final particles in their ground states. With all targets, states in ^{16}O with excitation energies of 9.83, 10.33, 11.04, 11.47, 11.98, 12.38, 12.98, 13.81 and 14.75 and 15.33 and 17.76 are populated. The spectra are almost identical for each target. There is a very close correspondence between the states observed in these data and those observed in $^{16}O(\alpha,\alpha')$ at 105 MeV [30]. A very preliminary analysis of the double differential cross sections using the empirical approach discussed in ref. [26] confirms further that the spins of the states excited in this experiment also have a one-to-one correspondence with those assigned in the $^{16}O(\alpha\ \alpha')$.

This correspondence suggests that the mechanism involved here is direct inelastic scattering. Further evidence comes from the angular distributions. We have analyzed the angular distribution for the 11.52 MeV level for reactions on ^{12}C and ^{13}C. These are shown in figure 10. Here $d\Omega^*$ is a solid element angle corresponding to the variables (θ^*, ϕ^*) and $d\Omega^*_\psi$ to the variables (ψ^*, χ^*).

Here we have binned the data as described in section 2 and plotted the double differential cross section as a function of $\langle\theta^*\rangle$ and $\langle\cos\psi^*\rangle$. Groups of data points for which $x-0.5 < \langle\cos\psi^*\rangle < x+0.5$ have been plotted together with a line drawn through them to guide the eye.

A strong diffractive structure is observed for both targets. This is conclusive evidence for the direct nature of the reaction mechanism. The shift of this diffractive structure with ψ^* is reproduced by DWBA calculations and can be used as an independent guide to the spin of the state [26].

It is not possible to make conclusive quantitative statements on the relative strength of excitation of states from a given E_{rel} spectrum. The total solid angle subtended in the center-of-mass frame varies rapidly as a function of E_{rel}, peaking somewhere near the center of the spectrum. In addition, as the analysis in ref. [26] shows, the double differential cross sections are considerably structured so that the count rate can vary rapidly as a function of θ_{HI} and θ_{LI}. Only general comments of a qualitative nature can be made.

For more negative Q-values we show in figure 11 typical spectra for the breakup of ^{16}O on ^{13}C. The data on ^{12}C and ^{28}Si are very similar. In these spectra we see a new peak at E_{rel} = 5.59 MeV which corresponds to a state in ^{16}O at 17.15 MeV that decays to the ^{12}C 4.44 MeV, 2+ level. The spectra in figure 11 for negative Q_3 gates show other notable features. We observe a peak at $E_{rel}\simeq 2.3$ MeV (channel 57) that can be associated with the decay of the 13.87 MeV state in ^{16}O to α + ^{12}C (4.44 MeV, 2+). Note also that the peak associated with the 11.10 MeV state in ^{16}O exhibits a low energy shoulder in the spectrum for $7.16<-Q_3<17.5$ MeV. This unresolved peak can be associated with a decay to the ^{12}C 4.44 MeV 2+ state, viz., that of the 15.41 MeV state in ^{16}O.

A feature of the spectrum corresponding to $17.5<-Q_3<27.5$ MeV is that only states at 9.85, 10.35, 11.10, 13.87 and 14.83 MeV are strongly excited while the state at 11.52 MeV is populated more weakly. This is to be contrasted with the results for $7.16<-Q3<17.3$ MeV. This is a feature which we have discussed previously in another publication [23]

Much of these negative Q-value data can thus be associated with the excitation of states at high excitation in ^{16}O which decay to excited states of ^{12}C and with mutual excitation involving both projectile and target nuclei. We anticipate that much of these data can therefore be explained by direct inelastic scattering.

Above the 4-body threshold, our data take the form of inclusive data for a quasi-3 body reaction where one of the nuclei might be $^{16}O^*$. ("quasi-3 body" implies that one nucleus is produced in an excited state which is particle unstable.) For example the continuum region could correspond to reaction in which an excited ^{20}Ne is formed which sequentially decays to $^{12}C+2\alpha$. Just as for true singles inclusive data we cannot reach any definite conclusions in this case.

3.1.2 The Breakup of ^{16}O into $^{15}N + p$

Other breakup channels are open for the inelastically excited ^{16}O nuclei produced in these reactions. In figure 12 we show (^{15}N,p) coincidence data for ^{12}C and ^{13}C targets.

We see for the Q_{ggg} spectra the same states as in $^{16}O^* \rightarrow {}^{12}C+\alpha$. The cross section for mutual excitation ($Q_3=Q_{ggg}-4.44$ MeV) on ^{12}C appears very small. The mutual excitation is stronger on ^{13}C ($Q_3=Q_{ggg}-3.68$ MeV). Here we see a triplet of narrow states at 12.99, 13.09 and 13.28 MeV. We associate these with some members of the T=1 quadruplet known at this excitation. This reaction is analogous to charge exchange (cf(^{16}O,^{16}N)) but with $\Delta T_Z=0$.

3.1.3 The α pickup reaction to ^{20}Ne

Q-value spectra for ^{16}O-α coincidences obtained with the ^{16}O beam on targets of ^{12}C, ^{13}C and ^{28}Si are shown in figure 13. In general the Q3 resolution, without the empirical corrections discussed in section 2, is not adequate to resolve states in the residual nuclei ^{8}Be, ^{9}Be and ^{24}Mg, respectively. However, in all spectra a strong broad peak is observed that corresponds to events in which the ^{16}O nucleus has been left in one of is excited states above 6 MeV. In figure 14, spectra of E_{rel} are shown for events in which the final state ^{16}O was left in its ground state. These spectra are qualitatively similar. States in ^{20}Ne are excited at 7.29, 8.49, 8.84, 10.16, 12.03, 12.64, 15.34, 16.70, and 17.23 MeV. In figure 15 we compare these α-^{16}O coincidence data from a ^{13}C target with singles data for the same reaction wth target and projectile interchanged, viz., $^{16}O(^{13}C,^{9}Be)^{20}Ne$. The similarity here indicates that α-transfer is the mechanism leading to ^{16}O-α coincidences via sequential breakup. Again further confirmation comes from a preliminary look at the double differential cross sections, which show diffractive structure and contain information on the spins of the states excited in ^{20}Ne. For more negative Q-values the data are consistent with the excitation of states in ^{20}Ne which decay to the 6 MeV states in ^{16}O. No statement can be made concerning the continuum.

3.1.4 Triton transfer, α decay

As a final example we show a spectrum of ^{15}N-α coincidences, for $Q=Q_{ggg}$. This spectrum (figure 16) shows peaks corresponding to states in ^{19}F. These states have also been seen in Li-induced 3-particle transfer reactions on ^{16}O [31]. Thus, the mechanism is probably direct three-particle transfer followed by particle decay.

In conclusion much of the data we have for breakup reactions induced by ^{16}O appears to arise from direct reactions, many of which have been studied by other means, followed by α decay or proton decay. It is not inconceivable that much of the continuum we see arises from direct reactions which excite states which will subsequently emit two particles. The kinematics of such reactions will be quite different from those of the single evaporation reactions both because of the greater recoil imparted to the heavy nucleus and because the decay correlations will be quite different. This possibility has not received a great deal of attention.

3.2 ^{20}Ne breakup into $^{16}O + \alpha$

Figure 17 shows the Q-value spectrum for the breakup of ^{20}Ne into $^{16}O+\alpha$. This spectrum has the same characteristics as these for ^{16}O breakup. In figure 17 we show the spectrum of E_{rel} for $Q=Q_{ggg}=-4.73$ MeV. Many states in ^{20}Ne are excited. These include states at 6.73, 7.16, 7.37, 7.78, 8.44, 8.79, 9.01, 9.44, 10.26, 10.80, 12.05, 12.72 and 15.37 MeV.

For ^{20}Ne there are no high resolution (α,α') data to compare with. Although the double differential cross sections for these data are too incomplete to make a detailed analysis (there is only one HI-α angle combination) they do show the same diffractive structure. Thus, the results are consistent with our overall picture of the reaction mechanisms involved. The advantages of using position sensitive detectors can be seen by comparing this spectrum wth those found in ref. [4].

4. Discussion and Conclusions

We have presented experimental results for the breakup of ^{16}O and ^{20}Ne on various light targets. We have discussed in detail the experimental techniques used to obtain high resolution. This experimental set-up is particularly well suited to study the sequential breakup mechanism. The data obtained are consistent with the mechanism for the

sequential component being direct in the first step and producing excited nuclei that subsequently decay by alpha-particle or proton emission. We would also expect substantial cross sections for direct reactions leading to excited states that decay by the sequential emission of two particles and thus contribute to the continuum in our spectra. Other possible origins of α-HI coincidences involving direct reactions are mutual inelastic excitation, in which both nuclei are above particle thresholds, and transfer reactions on to the target. The latter can produce light particles either from the target (by excitation of particle unstable states) or from the ejectile (which could also be left in a particle unstable state.)

Similar measurements of ^{18}O on ^{12}C have shown that the double-differential cross sections for these direct reactions are complex - although they display a simple systematics and are well predicted by DWBA and the Strong Absorption Model [26]. Clearly these cross sections must be understood in order to identify and account for sequential breakup in searches for other reaction mechanisms.

Finally we remark that the technique presented here provides a very powerful tool for studies of direct reactions with heavy ions. The high resolution combined with the spin and reaction mechanism information that can be obtained from the double-differential cross sections [26] make it an attractive technique. Indeed such a program is underway at the NSF Daresbury where the technique is referred to as Resonant Particle Spectroscopy [32].

We would like to thank Dr. R. K. Bhowmik for many fruitful discussions and for help in the analysis of the angular distributions. This work was supported by the Director, Office of Energy Research, Division of Nuclear Physics of the Office of High Energy and Nuclear Physics of the U.S. Department of Energy under Contract DE-AC03-76SF00098.

REFERENCES

1. C. K. Gelbke et al., Phys. Lett. 71B, 83 (1977)
2. M. Bini et al., Phys. Rev. 22C, 1945 (1980)
3. A. Gamp et al., Z. Phys. 300A 63 (1981)
4. H. Homeyer et al., Phys. Rev. 26C 1335 (1982)
5. R. K. Bhowmik et al., Nucl. Phys. A390 117 (1982)
6. T. C. Awes et al., Phys. Rev. 25C 2361 (1982)
7. H. Homeyer et al., Z. Phys. 314A 143 (1983)
8. H. Ryde, Physica Scripta T5 114 (1983)
9. H. Homeyer, Conference on Nuclear Physics with Heavy Ions, Stony Brook, New York, Apr 1983.
10. Ch. Egelhaaf et al., to be submitted to Nucl. Phys.
11. D. M. Brink, Phys. Lett. 40B 37 (1972)
12. P. J. Siemens et al., Phys. Lett 36B 24 (1971)
13. J. Wilczynski et al., Phys. Rev. Lett. 45 606 (1980)
14. B. G. Harvey and M. J. Murphy, Phys. Lett 130B 373 (1983)
15. B. G. Harvey and H. Homeyer, LBL Report 16882 (Nov 1983), submitted to Phys. Rev. Lett.
16. W. A. Friedman, Phys. Rev. 27C 569 (1983)
17. K. W. McVoy and M. C. Nemes, Z. Physik 295A 177 (1980)
18. M. Blann, Phys. Rev. C23 205 (1981)
19. N. Stelte et al., Nucl. Phys. A384 190 (1982)
20. W. G. Lynch et al., Phys. Rev. Lett 51 1850 (1983)
21. A. C. Shotter et al., Phys. Rev. Lett. 46 12 (1981)
22. W. D. Rae et al., Phys. Rev. Lett. 45 884 (1980)
23. W. D. Rae et al., Phys. Lett. 105B 417 (1981)
24. J. Van Driel, et al., Phys. Lett. 98B 351 (1981)
25. M. Sasagase, et al., Phys. Rev. C27 2630 (1983)
26. W. D. M. Rae and R. K. Bhowmik, to be published in Nucl. Phys. A.
27. J. T. Walton, F. S. Goulding, E. E. Haller and R. H. Pehl, Nucl. Instr. and Meth. 196 107 (1982)
28. L. C. Northcliffe and R. F. Schilling, Nuclear Data Tables, A7, 233 (1970)
29. H. Fuchs, Nucl. Inst. and Meth. 200 361 (1982)

30. M. N. Harekh, et al., Nucl. Phys. A265 189 (1976)
31. L. M. Martz, et al., Phys. Rev. C20 1340 (1979)
32. W. D. Rae, et al., SERC Daresbury Annual Report 1982/83, Nuclear Structure Appendix, p. 13.
33. H. S. Bradlow, et al., Nucl. Phys. A314, 171 (1979)

Figure Captions

Fig. 1 Schematic of experimental setup. The light-ion telescope detected p, d, t, ^{3}He and ^{4}He.

Fig. 2 A typical position spectrum from the E detector of the α telescope with calibration grids in position. The grid consisted of 1 mm diameter holes spaced 2 mm apart. One aperture was reduced in area for identification.

Fig. 3 A schematic Q_3 spectrum illustrating the various possible components.

Fig. 4 A schematic illustration of the ambiguity in associating peaks in the E_{rel} spectrum with a unique excitation energy in the ejectile. The schematic spectrum a) corresponds to final states in which all three particles were produced in their ground states. These events may be selected by requiring $Q_3 = Q_{ggg}$. At more negative Q-values it may not be possible to determine from the measured Q-value above (because of finite experimental resolution) whether the detected heavy ion was produced in its ground state. In this case additional peaks, as indicated by the shaded areas in b) and corresponding to excited states of the detected heavy ion, enter the spectrum of E_{rel} and may cause ambiguities in the determination of the excitation energy of the ejectile.

Fig. 5 Two different decay configurations used to discuss the various contributions to the E_{rel} resolution.

Fig. 6 Definition of the angles used in determining the cross sections.

Fig. 7 The relation between cuts in the angle ψ and the detector energy threshold and angle threshold. Cross section calculations near ψ_1 and ψ_2 are unreliable.

Fig. 8 Q_3 spectra for ^{16}O $^{12}C + \alpha$ on targets of ^{12}C, ^{13}C and ^{28}Si.

Fig. 9 E_{rel} spectra for ^{16}O $^{12}C + \alpha$ for $Q_3 = -7.16$ MeV on targets of ^{12}C, ^{13}C and ^{28}Si.

Fig. 10 Angular distribution for inelastic excitation of ^{16}O to 11.52 MeV. Here θ^* is the center-of-mass angle of the $^{16}O^*$ and ψ^* is the angle of $\vec{v}_{rel}$ with respect to the $^{16}O^*$ direction in the lab. The sets of data inserted with $\langle\cos\psi^*\rangle = x$ corresponding to data sets for $x-0.5 < \langle\cos\psi^*\rangle < x+0.5$. The lines are to guide the eye.

Fig. 11 E_{rel} spectra fr $^{16}O \rightarrow {}^{12}C + \alpha$ on ^{13}C target for negative Q_3 bins.

Fig. 12 E_{rel} spectra for $^{16}O \rightarrow {}^{15}N+p$ on ^{12}C and ^{13}C.

Fig. 13 Q_3 spectra for $^{16}O-\alpha$ coincidences with ^{16}O beam on ^{12}C, ^{13}C and ^{28}Si.

Fig. 14 E_{rel} spectra for $^{20}Ne \rightarrow {}^{16}O + \alpha$ coincidences with ^{16}O beam. The final ^{16}O is in its ground state.

Fig. 15 A comparison of $\alpha - {}^{16}O$ coincidence data on a ^{13}C target with singles data (ref. [33]) for the same reaction with target and projectile reversed.

Fig. 16 E_{rel} for $^{15}N-\alpha$ coincidences. All final particles are in their ground state.

Fig. 17 Q_3 spectrum for $^{20}Ne \rightarrow {}^{16}O + \alpha$ in ^{20}Ne breakup on a ^{12}C target.

Fig. 18 E_{rel} spectrum for $^{20}Ne \rightarrow {}^{16}O+\alpha$. All final particles are in their ground state.

Schematic diagram of experimental setup

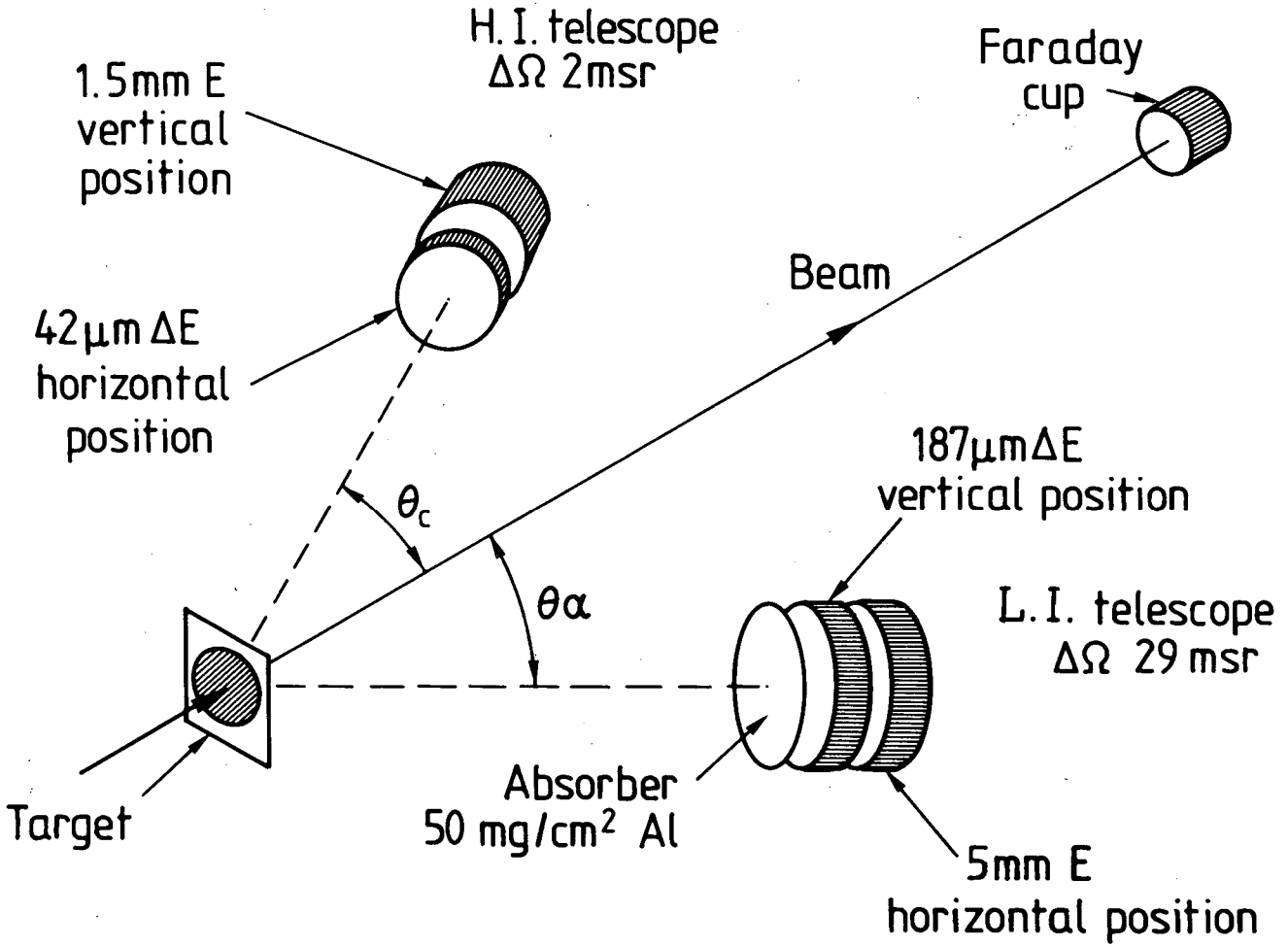

XBL 842-854

Fig. 1

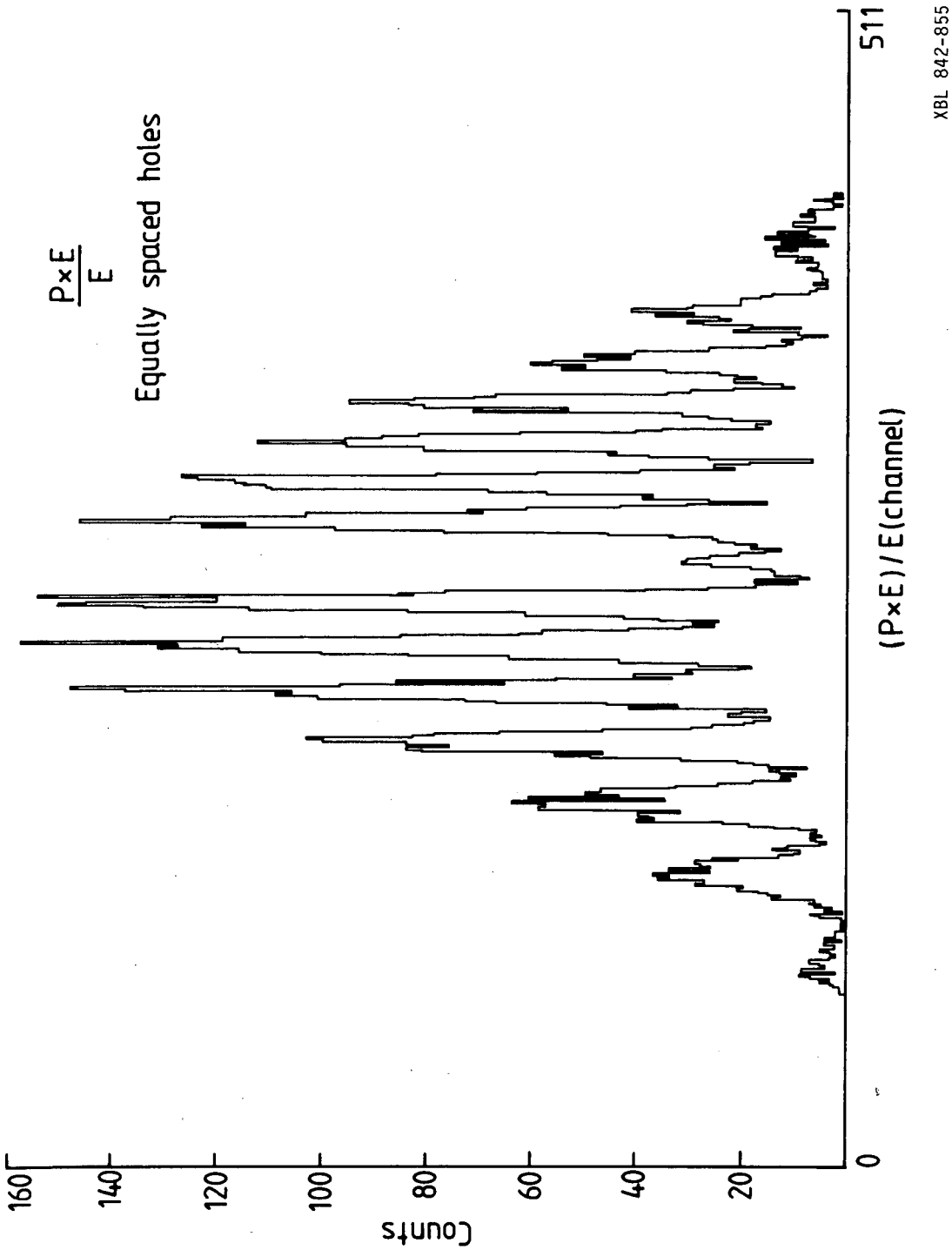
P×E / E
Equally spaced holes
Counts
160
140
120
100
80
60
40
20
0
511
(P×E) / E(channel)
XBL 842-855

Fig. 2

Total reaction Q - value

$$Q_3 = K.E._{beam} - K.E._{heavy\ particle} - K.E._{light\ particle} - K.E._{residual}$$

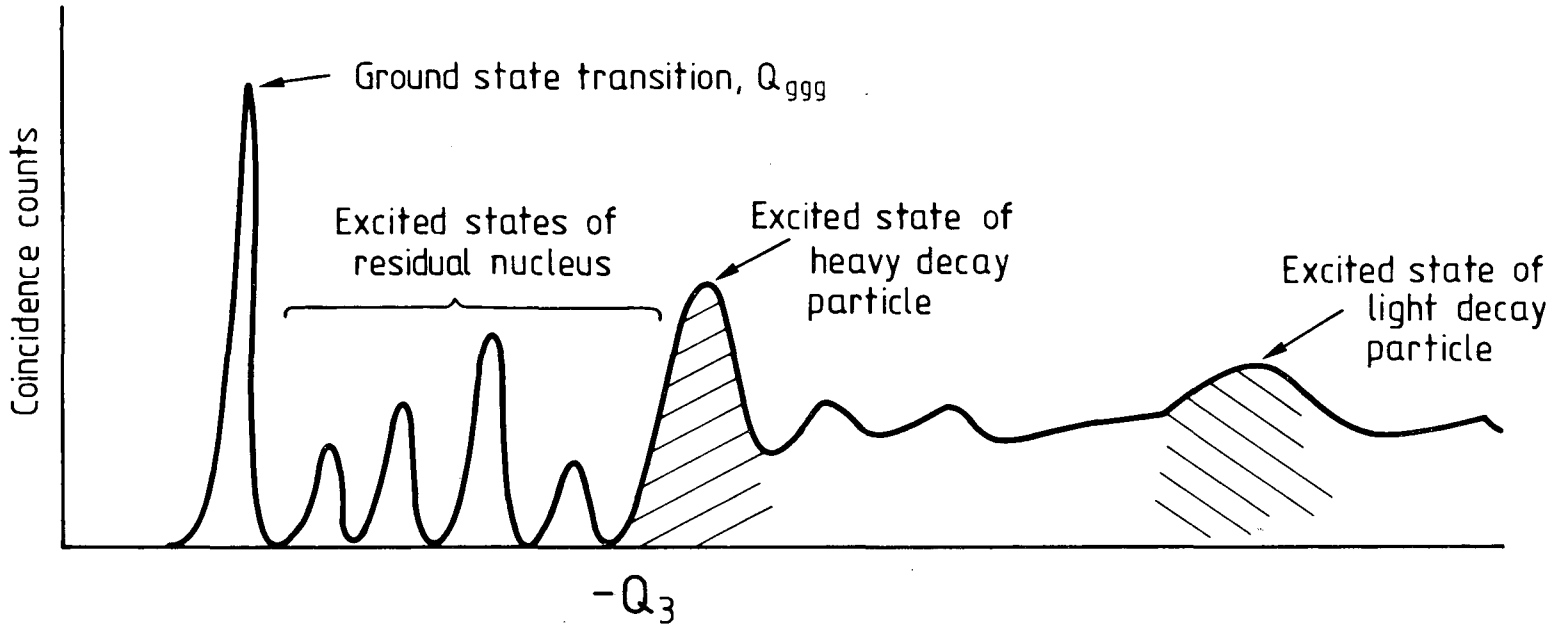

XBL 842-856

Fig. 3

Relative kinetic energy of decay products

$$E_{rel} = \text{Kinetic energy released in decay} = \frac{1}{m_H + m_L}\left\{m_H E_L + m_L E_H - 2\sqrt{m_L m_H E_L E_H}\cos\Theta\right\}$$

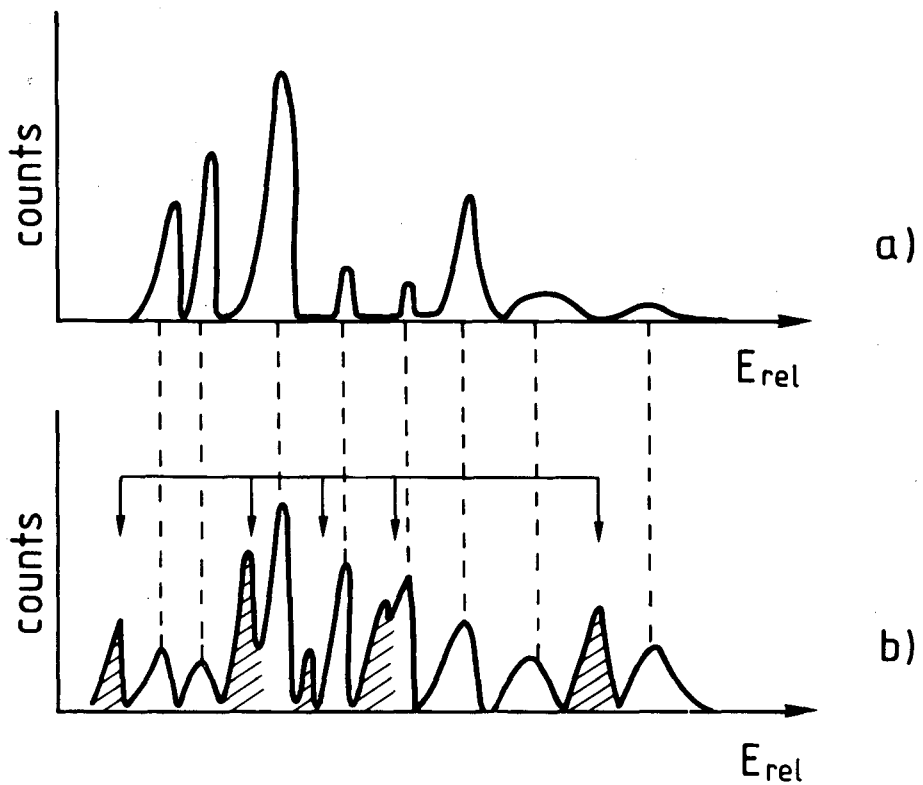

XBL 842-857

Fig. 4

E_{rel} resolution

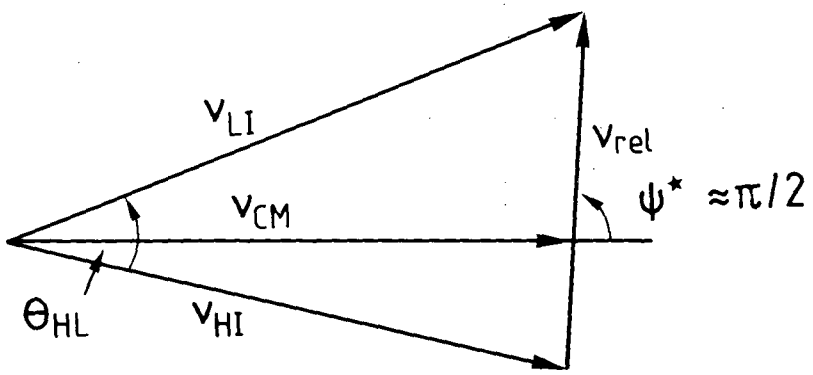

Configuration a)

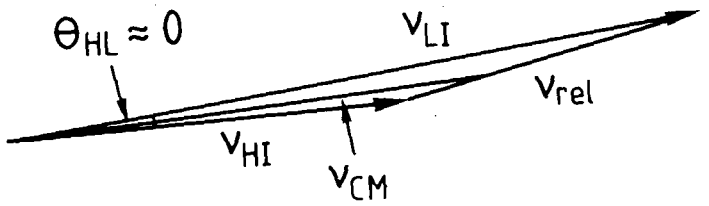

Configuration b)

XBL 842-858

Fig. 5

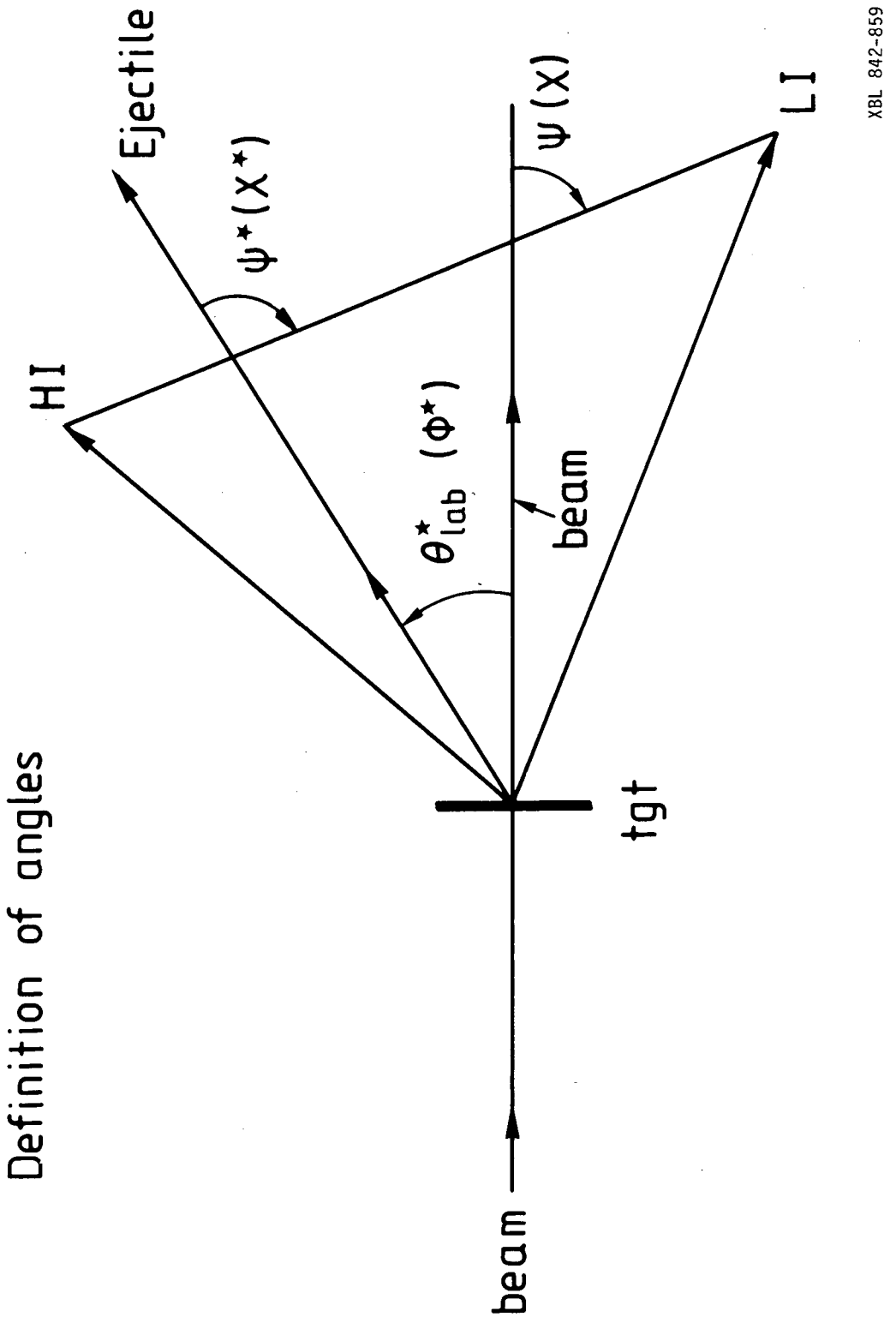
Definition of angles
Ejectile
HI
LI
$\psi^*(X^*)$
$\psi(X)$
θ^*_{lab} (Φ^*)
beam
tgt
beam
XBL 842-859

Fig. 6

Data analysis

a) Angle bins

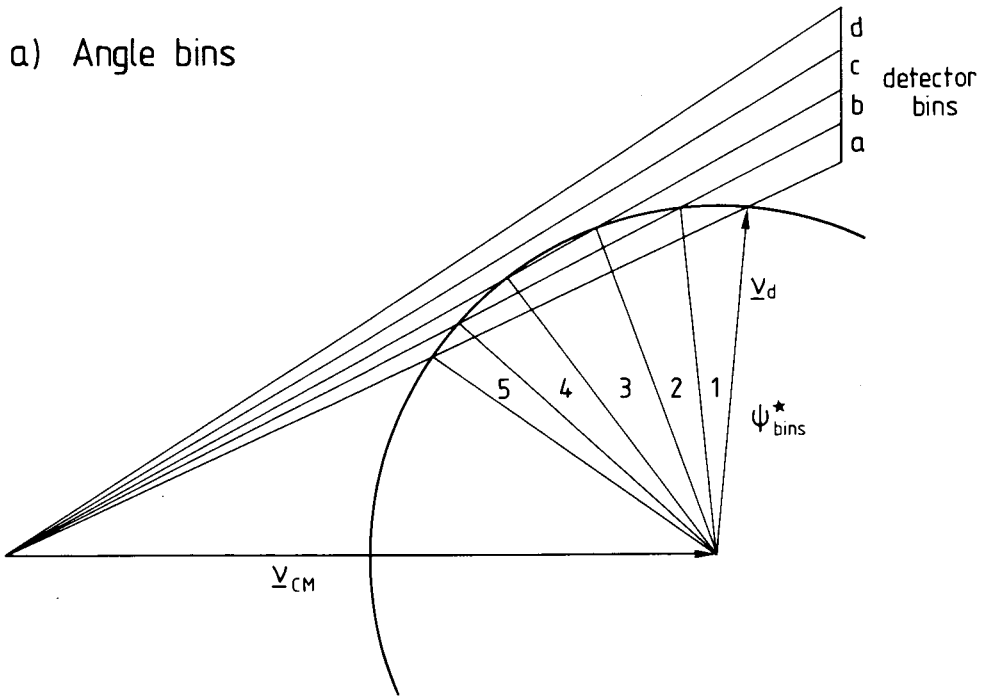

b) Energy thresholds

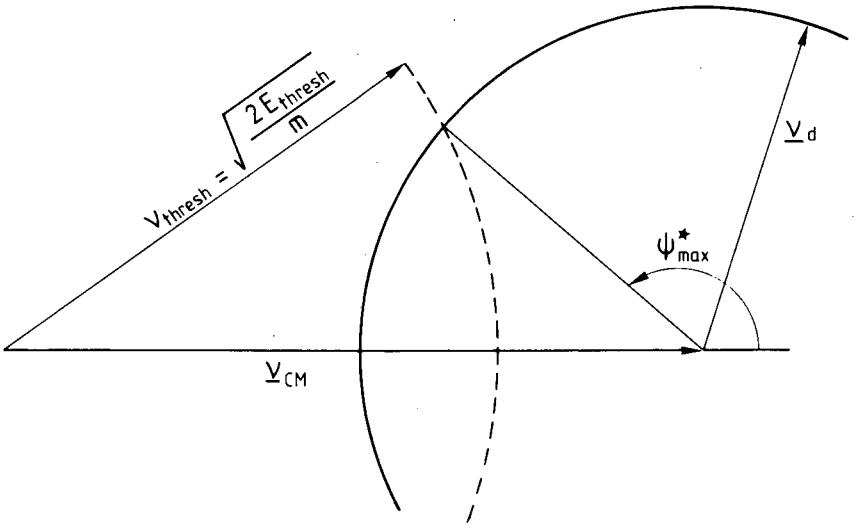

XBL 842-860

Fig. 7

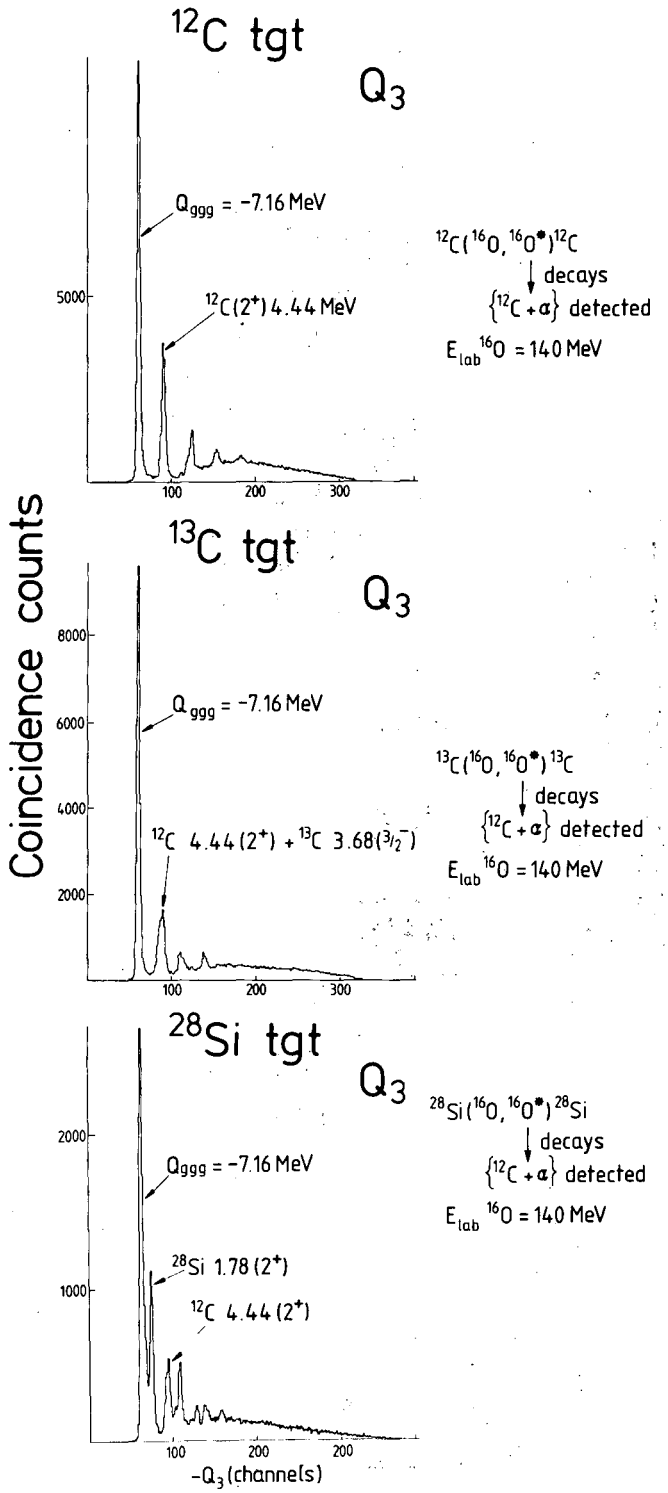

XBL 842-861

Fig. 8

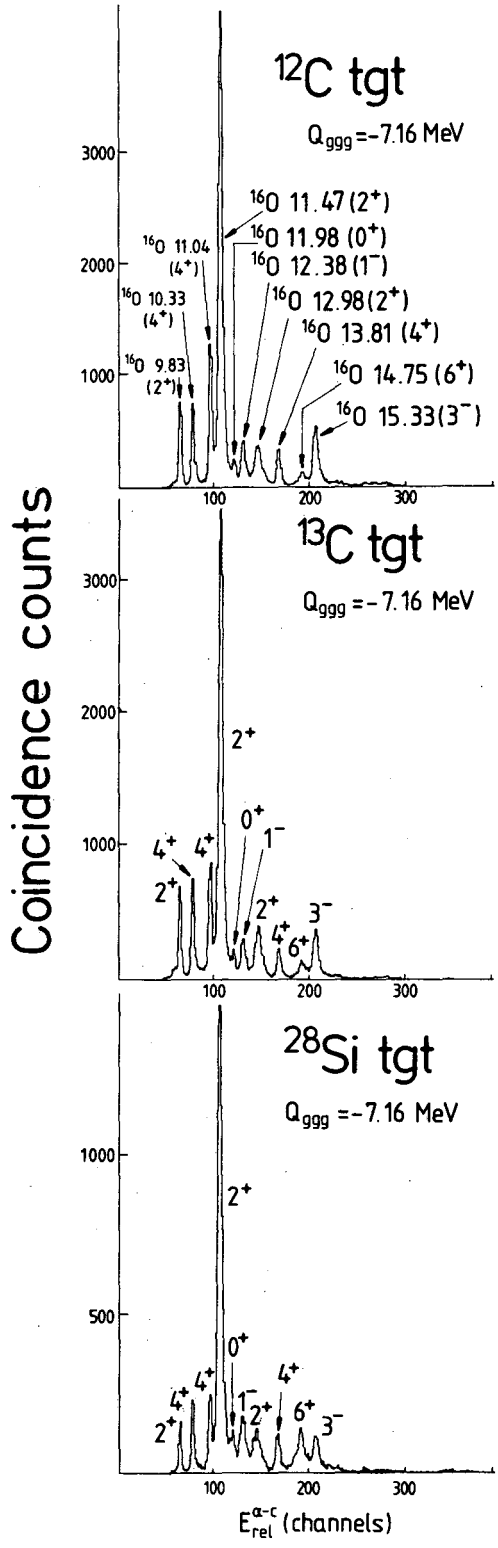

XBL 842-862

Fig. 9

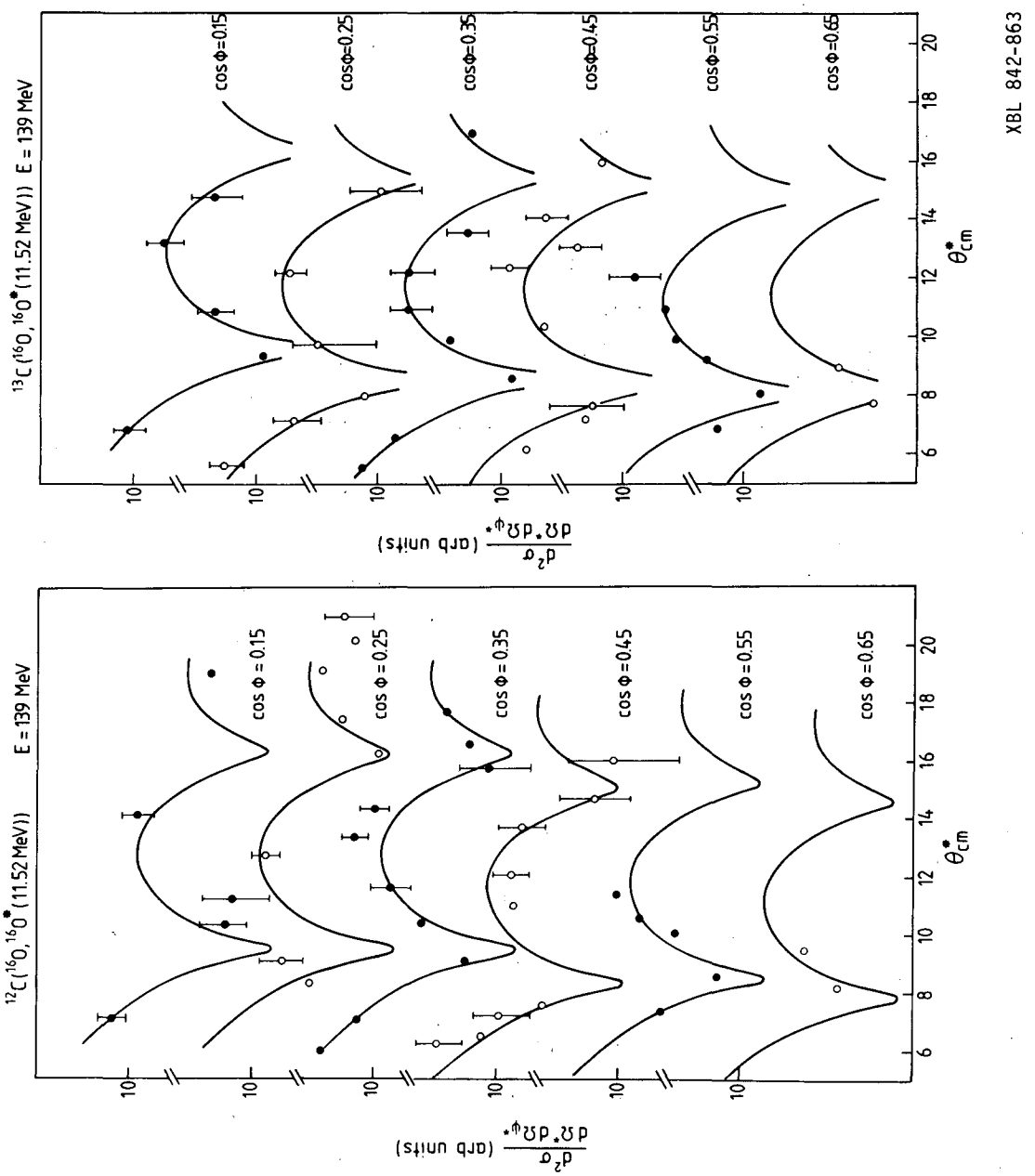

XBL 842-863

Fig. 10

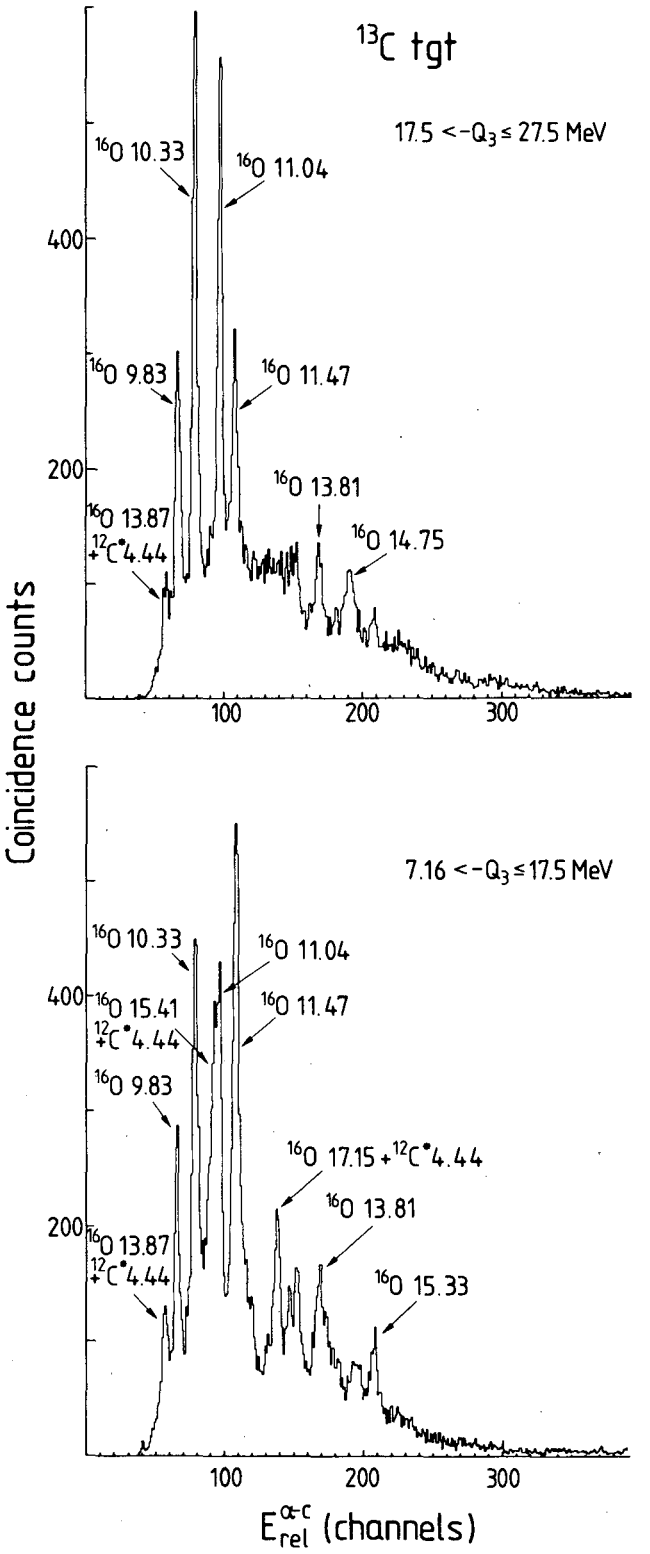

XBL 842-864

Fig. 11

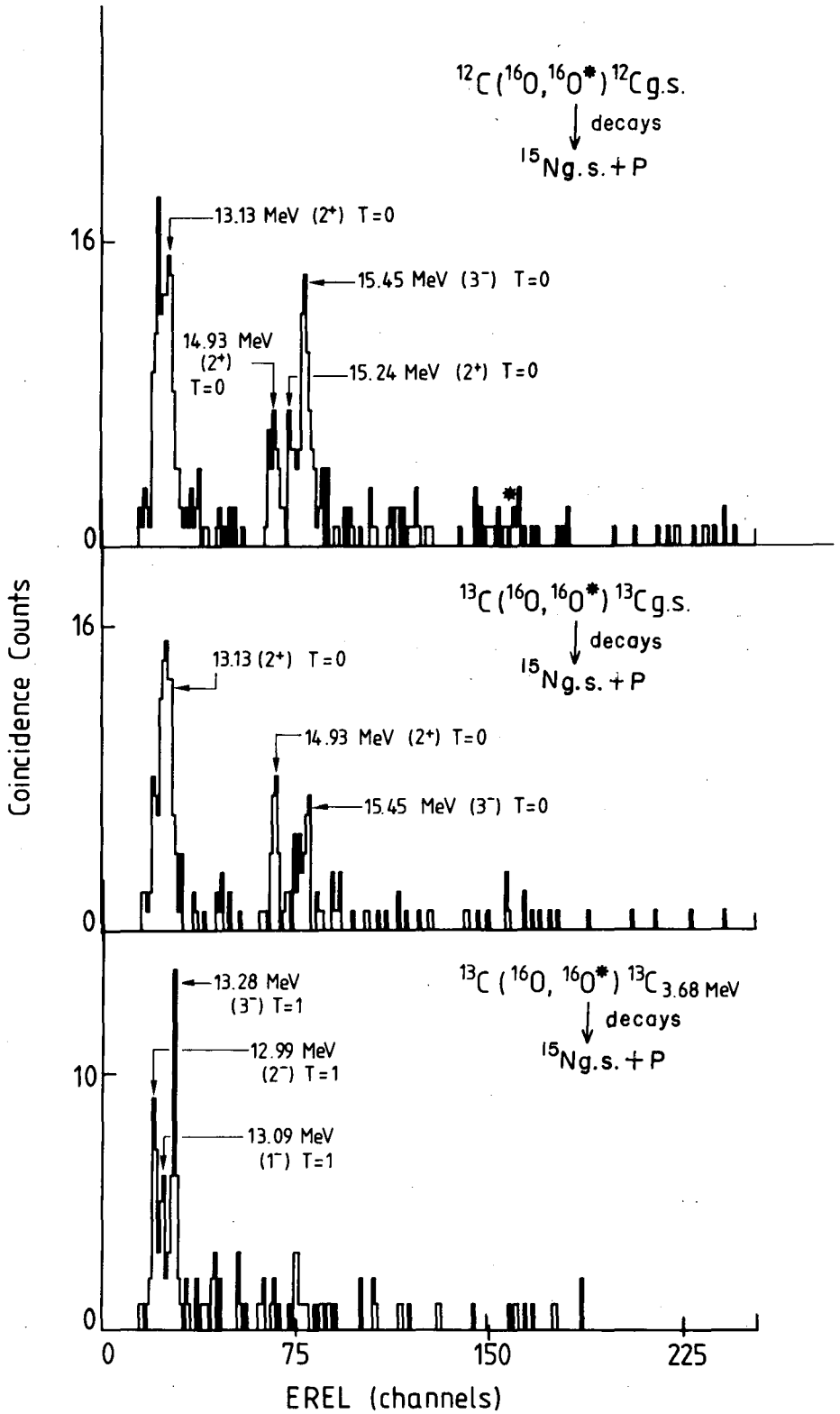

XBL 842-865

Fig. 12

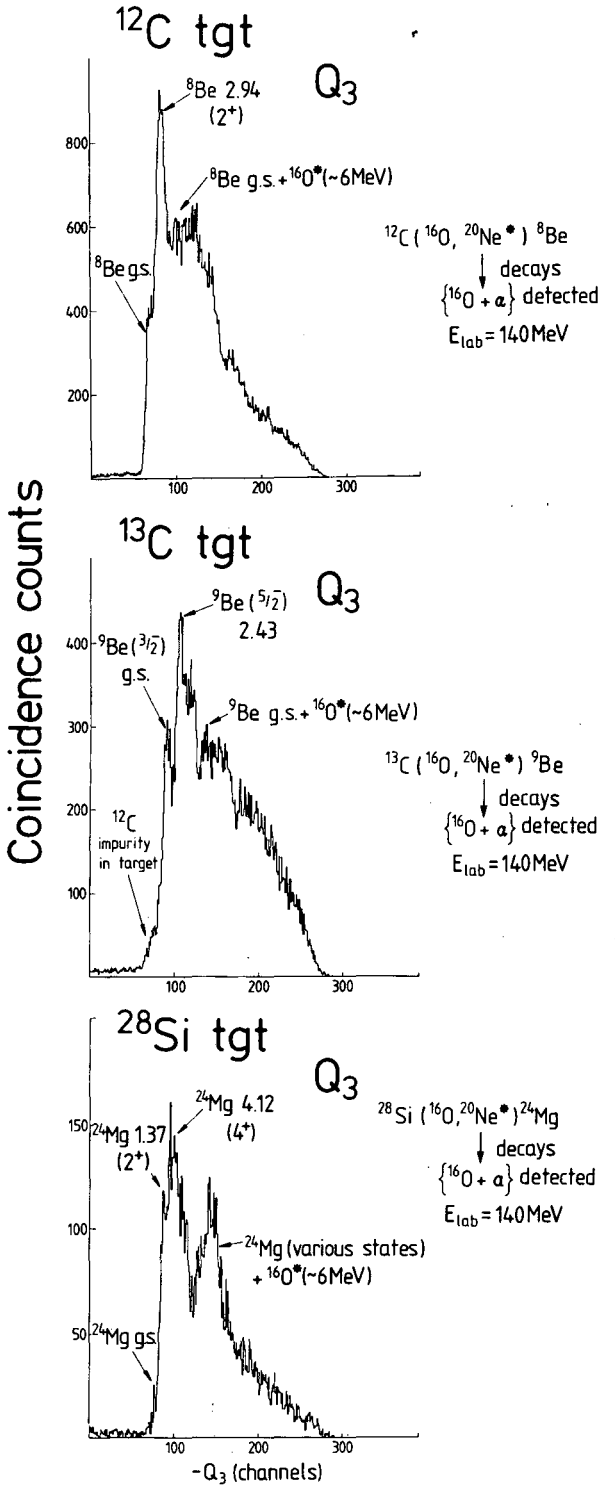

XBL 842-866

Fig. 13

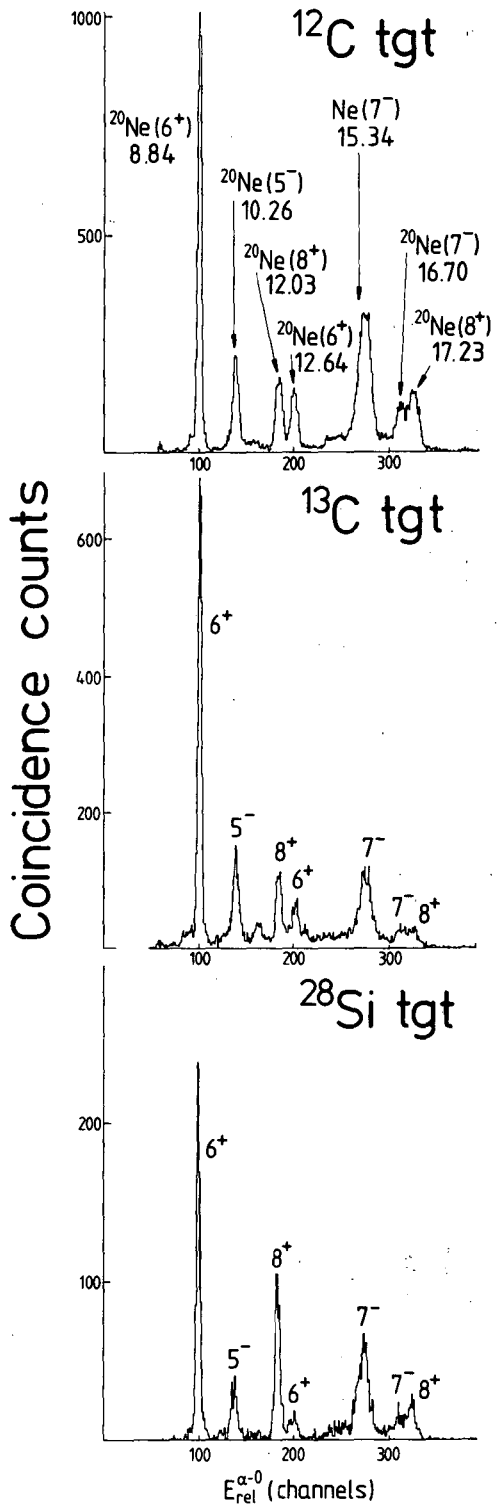

XBL 842-867

Fig. 14

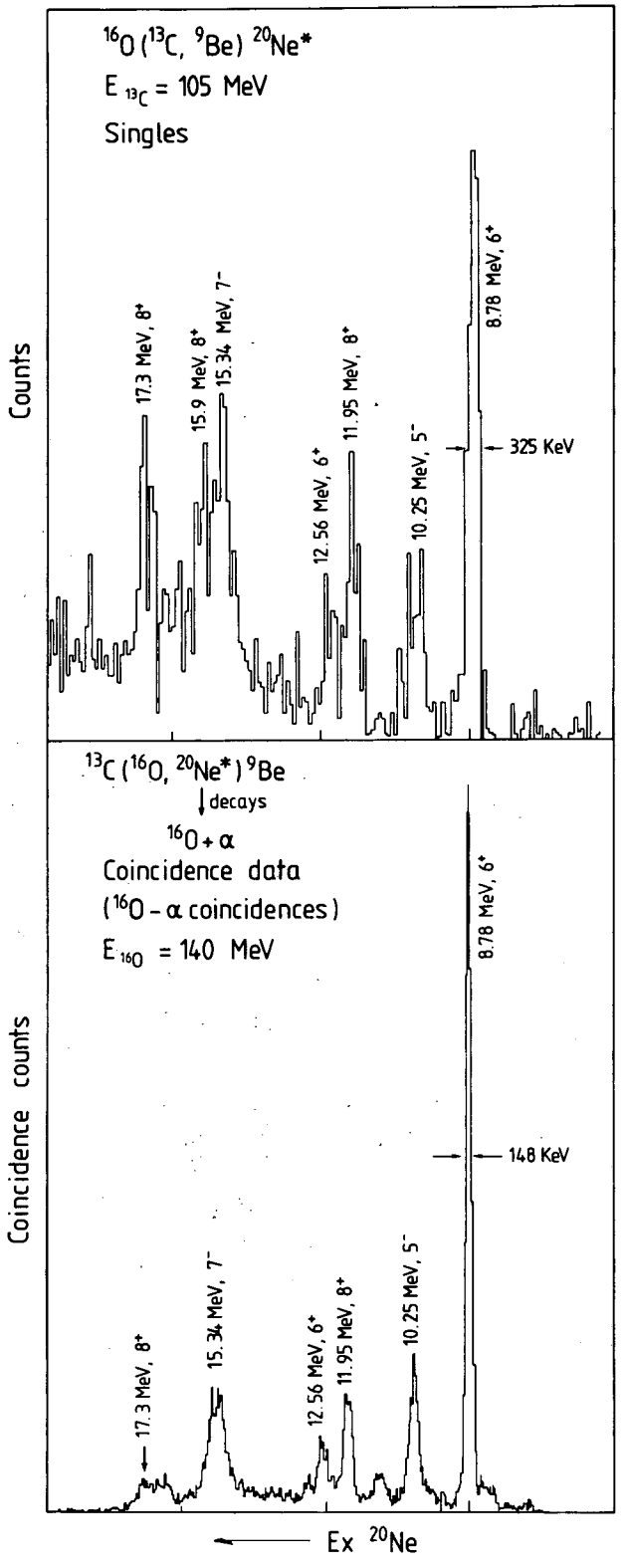

XBL 842-868

Fig. 15

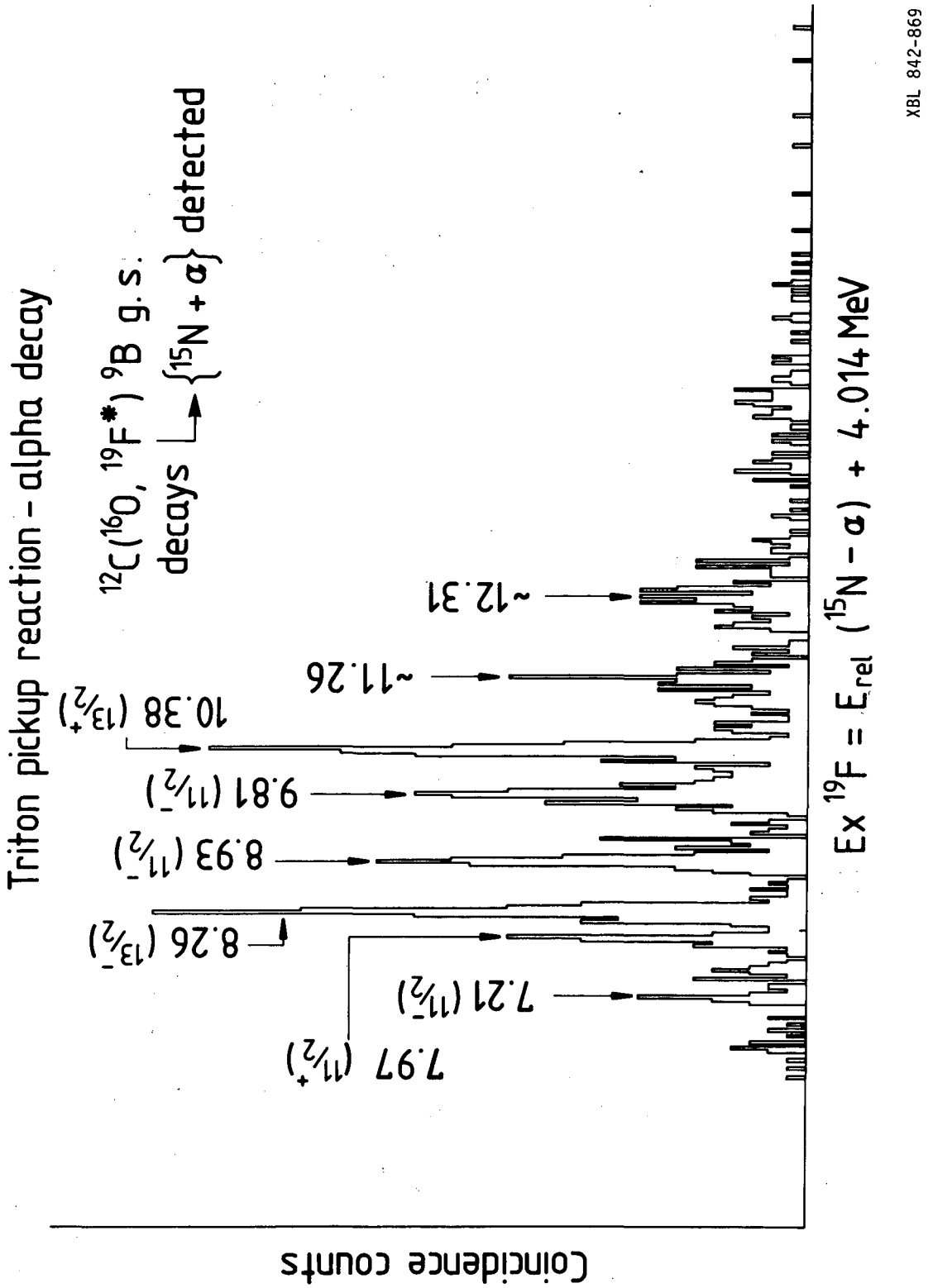
Triton pickup reaction - alpha decay
$^{12}C(^{16}O, ^{19}F^*)\ ^9B$ g.s.
decays $\{^{15}N + \alpha\}$ detected
~12.31
~11.26
10.38 ($13/2^+$)
9.81 ($11/2^-$)
8.93 ($11/2^-$)
8.26 ($13/2^-$)
7.21 ($11/2^-$)
7.97 ($11/2^+$)
Ex $^{19}F = E_{rel}$ ($^{15}N - \alpha$) + 4.014 MeV
Coincidence counts
XBL 842-869

Fig. 16

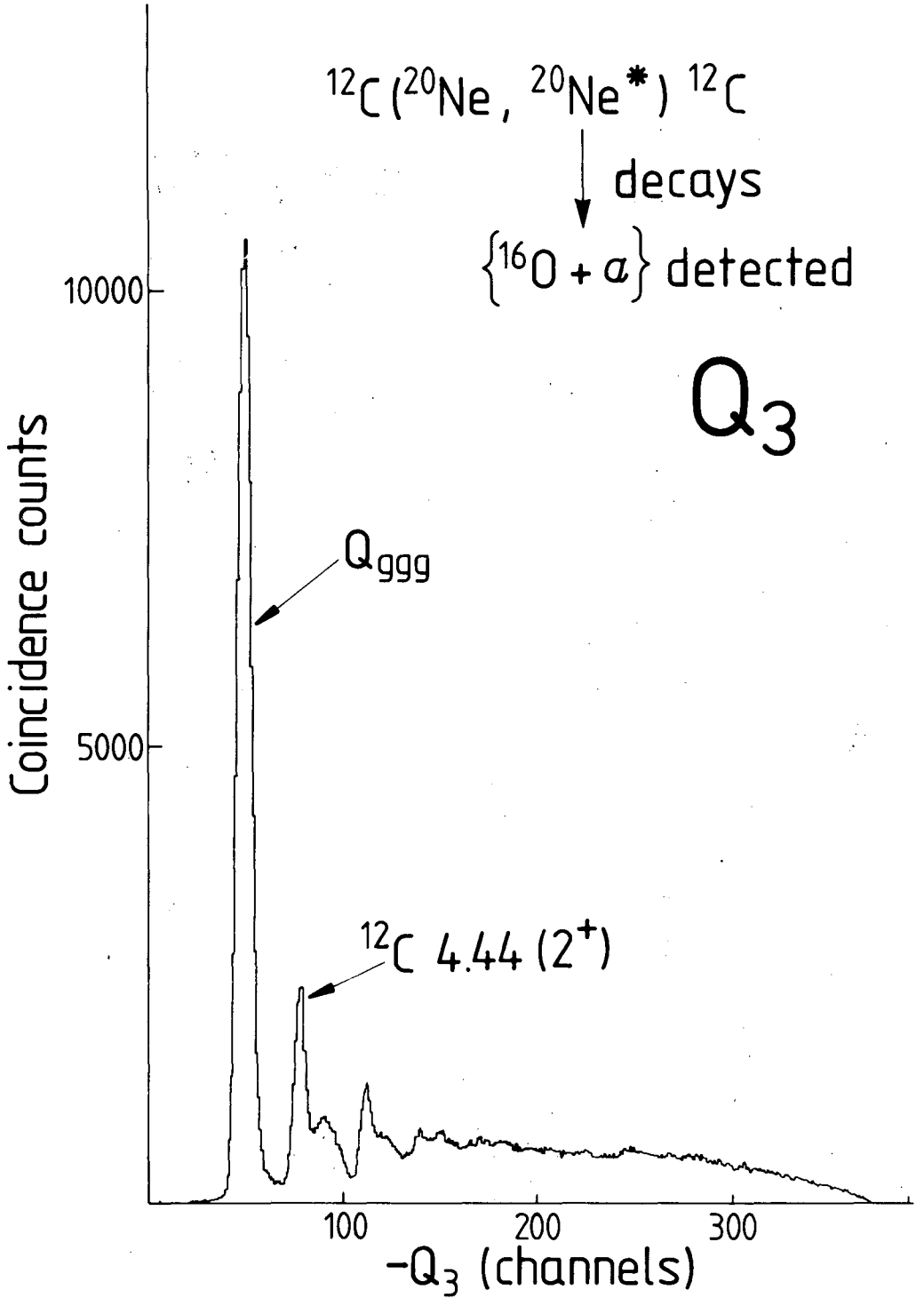

XBL 842-870

Fig. 17

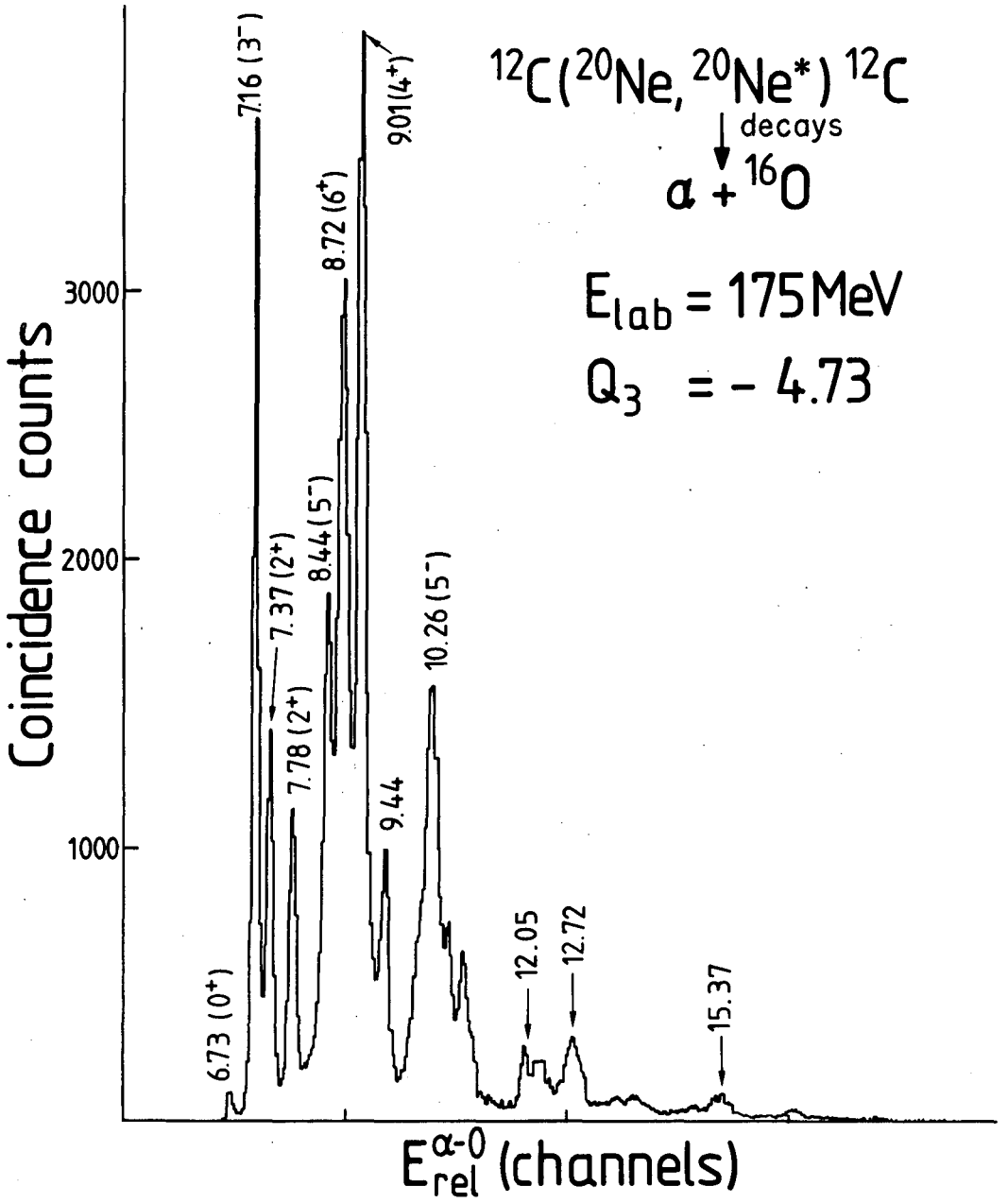

XBL 842-871

Fig. 18

This report was done with support from the Department of Energy. Any conclusions or opinions expressed in this report represent solely those of the author(s) and not necessarily those of The Regents of the University of California, the Lawrence Berkeley Laboratory or the Department of Energy.

Reference to a company or product name does not imply approval or recommendation of the product by the University of California or the U.S. Department of Energy to the exclusion of others that may be suitable.

TECHNICAL INFORMATION DEPARTMENT
LAWRENCE BERKELEY LABORATORY
UNIVERSITY OF CALIFORNIA
BERKELEY, CALIFORNIA 94720